

Chapter 7

Krypton Adsorption on Zeolite-Templated Carbon and Anomalous Surface Thermodynamics

M. Murialdo, N.P. Stadie, C.C. Ahn, and B. Fultz, "Krypton Adsorption on Zeolite-Templated Carbon and Anomalous Surface Thermodynamics," *Langmuir*, 31, 7991 (2015).

DOI: 10.1021/acs.langmuir.5b01497

<http://pubs.acs.org/doi/abs/10.1021/acs.langmuir.5b01497>

Abstract

Krypton adsorption was measured at 8 temperatures between 253 and 433 K on a zeolite-templated carbon and two commercial carbons. The data were fitted using a generalized Langmuir isotherm model and thermodynamic properties were extracted. Differing from that on commercial carbons, krypton adsorption on the zeolite-templated carbon is accompanied by an increasing isosteric heat of adsorption, rising by up to 1.4 kJ mol^{-1} as a function of coverage. This increase is a result of enhanced adsorbate-adsorbate interactions promoted by the ordered, nanostructured surface of the adsorbent. An assessment of the strength and nature of these adsorbate-adsorbate interactions is made by comparing the measured isosteric heats of adsorption (and other thermodynamic quantities) to fundamental metrics of intermolecular interactions of krypton and other common gases.

1. Introduction

High surface area carbon materials have garnered interest for a variety of adsorptive applications^{1,2,3,4} ranging from hydrogen storage^{5,6} to carbon capture^{7,8} and many others. The recently emerged class of templated carbon materials^{9,10,11} exhibiting controlled pore-size distributions that depend on the template, have shown exceptional performance in many adsorptive applications owing to their uniquely ordered structure. Zeolite-templated carbon (ZTC) is one of the highest surface area carbonaceous materials known¹², and therefore exhibits a high specific adsorptive capacity toward small molecular species including hydrogen^{13,14} nitrogen¹⁵, carbon dioxide¹⁶, methane¹⁷, and water¹⁸. Further, our recent work has shown that ZTC exhibits not only a high specific adsorptive capacity, but also hosts an adsorbed phase with highly unusual properties; both ethane¹⁹ and methane²⁰ exhibit isosteric heats of adsorption on ZTC that *increase* with increasing surface coverage, a particularly rare and advantageous property for deliverable storage capacity. Due to its chemical homogeneity²⁰ and narrow pore-size distribution centered at a width of 12 Å, the surface of ZTC is optimized for promoting lateral interactions between adsorbed molecules, even when these interactions are exceedingly weak (e.g., as for methane).

Krypton, the fourth noble gas, is an unreactive monatomic gas that otherwise bears many similarities to methane. The two gases share a similar size (Kr: 3.9 Å, CH₄: 4.0 Å)²¹ and approximately spherical symmetry, as well as similar boiling points (120 K and 112 K, respectively)²² and critical temperatures (209 K and 190 K, respectively)²². Conveniently, monatomic krypton allows for very simple calculations of thermodynamic properties such as entropy, since rotational and internal vibrational modes do not exist. Krypton has applications in the photography, lighting²³, and medical industries,^{24,25} and is commonly used as an

adsorbate for characterizing low-surface-area materials^{26,27}. There is also active interest in finding adsorbent materials that can effectively separate krypton from xenon, especially the radioactive isotope ^{85}Kr .^{28,29} These gases are off-gassed from spent nuclear fuel and their separation is crucial to the development of “closed” nuclear fuel cycles³⁰. Nevertheless, krypton adsorption across a wide range of temperatures and pressures is a relatively unexplored topic, and the results can have relevant implications for many other more complex adsorptive systems.

2. Experimental

2.1 Materials Synthesis

Three microporous carbons were chosen for this study: MSC-30, CNS-201 and ZTC. MSC-30 was obtained from Kansai Coke & Chemicals Company Ltd. (Japan) and CNS-201 was obtained from A. C. Carbone Inc. (Canada). ZTC is a zeolite-templated carbon that was synthesized in a multistep process³¹ based on a previously reported approach designed to achieve high template fidelity of the product¹³. The template used was a NaY zeolite (faujasite) obtained from Tosoh Corp. (Japan). Briefly, the zeolite was first impregnated with furfuryl alcohol, which was polymerized at 423 K, before undergoing a 973 K propylene chemical vapor deposition step, and finally carbonization at 1173 K. The zeolite template was removed by dissolution in 48% hydrofluoric acid. The synthesis is described in detail elsewhere³¹.

2.2 Materials Characterization

Nitrogen adsorption isotherms were measured at 77 K using a BELSORP-max instrument (BEL-Japan Inc.). From these measurements, micropore volumes (Dubinin-

Radushkevich (DR) method^{32,33}) and specific surface areas (Brunauer-Emmett-Teller (BET) method³⁴) were determined. Pore-size distributions were obtained using non-local density functional theory (NLDFI) analysis^{35,36} with a carbon slit-pore model and software from Micromeritics Instrument Corp. The skeletal density of each material was determined by helium pycnometry.

2.3 Measurements

Equilibrium adsorption isotherms of krypton on the three carbon adsorbents were measured at 8 temperatures between 253 and 433 K. Research-grade krypton (99.998%) was obtained from Air Liquide America Corp. and used in a custom Sieverts apparatus designed and tested for accuracy up to 10 MPa.³⁷ Measurements were made up to high pressures using an MKS Baratron (Model 833) pressure transducer. Each of the samples was degassed at 520 K under a vacuum of less than 10^{-9} MPa prior to testing. The Sieverts was equipped with a molecular drag pump capable of achieving a vacuum of 10^{-10} MPa and vacuum pressures were verified using a digital cold cathode pressure sensor (I-MAG, Series 423). The adsorbent was loaded into a stainless steel reactor, sealed with a copper gasket, and held at a constant temperature. To obtain low temperature isotherms, the reactor was submerged in a circulated chiller bath with temperature fluctuations no larger than ± 0.1 K. High temperature isotherms were obtained by encasing the reactor in a copper heat exchanger wrapped with insulating fiberglass heating tape. Using a PID controller, the reactor temperature was maintained with fluctuations no larger than ± 0.4 K. The temperature of the reactor was monitored with K-type thermocouples while the temperature of the gas manifold was measured with platinum resistance thermometers. For calculations of excess uptake, bulk phase gas densities were obtained from the REFPROP Standard Reference Database²². Multiple adsorption/desorption

isotherms were taken to ensure complete reversibility and identical measurements were found to be reproducible to within 1% error.

3. Results

3.1 Adsorbent Characterization

The BET surface areas of ZTC, MSC-30, and CNS-201 were determined to be 3591 ± 60 , 3244 ± 28 , and 1095 ± 8 $\text{m}^2 \text{g}^{-1}$, respectively. ZTC and MSC-30 also have similar micropore volumes of 1.66 and 1.54 $\text{cm}^3 \text{g}^{-1}$ while CNS-201 has a much smaller micropore volume of 0.45 $\text{cm}^3 \text{g}^{-1}$. Despite their similarities, ZTC and MSC-30 have very different pore-size distributions (Figure 1). Due to its templated nature, ZTC exhibits a single, sharp peak in its pore-size distribution, corresponding to a pore width of 12 Å. This has been determined by NLDFT pore-size analysis and further evidence is given by X-ray diffraction and transmission electron microscopy (TEM) investigations²⁰. Based on NLDFT pore-size analysis, over 90% of the micropore volume of ZTC is contained in pores with widths between 8.5 and 20 Å. MSC-30 on the other hand has a broad pore-size distribution with micropore widths ranging from 6 to 35 Å and over 40% of its micropore volume is in pores of widths greater than 21 Å. CNS-201, has three prominent pore widths at approximately 5.4, 8.0, and 11.8 Å, which contain roughly 50%, 20%, and 15% of the micropore volume respectively. The skeletal density of both activated carbons (MSC-30 and CNS-201) was found to be 2.1 g cm^{-3} , which is close to the ideal density of graphite ($\sim 2.2 \text{ g cm}^{-3}$). The templated carbon ZTC, however, was found to have a skeletal density of 1.8 g cm^{-3} , which is in agreement with other zeolite-templated carbons.^{20,31}

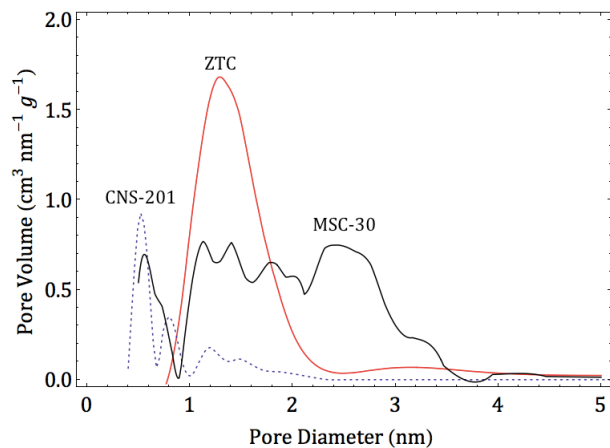


Figure 1. Pore-size distributions of the three carbon materials (CNS-201, MSC-30, and ZTC) derived from NLDFT analysis of nitrogen adsorption measurements at 77 K.

3.2 Adsorption Measurements

Equilibrium excess adsorption isotherms of krypton on ZTC, MSC-30 and CNS-201 are presented in Figure 2. At high pressures and low temperatures, excess adsorption reaches a maximum, a well-known phenomenon for Gibbs excess adsorption³⁸. At 253 K, ZTC, MSC-30, and CNS-201 have excess adsorption maxima of 22.6, 23.3, and 7.9 mmol g⁻¹, respectively. At 298 K, the excess adsorption maxima are 16.3, 17.7, and 6.6 mmol g⁻¹, respectively. MSC-30 exhibits a greater excess adsorption maximum than ZTC at all temperatures measured. This is in contrast to methane adsorption on the same materials where excess adsorption quantities on ZTC exceeded those on MSC-30 at low temperatures (238-265 K). CNS-201 exhibits the smallest excess adsorption uptake of the three materials due to its lower surface area.

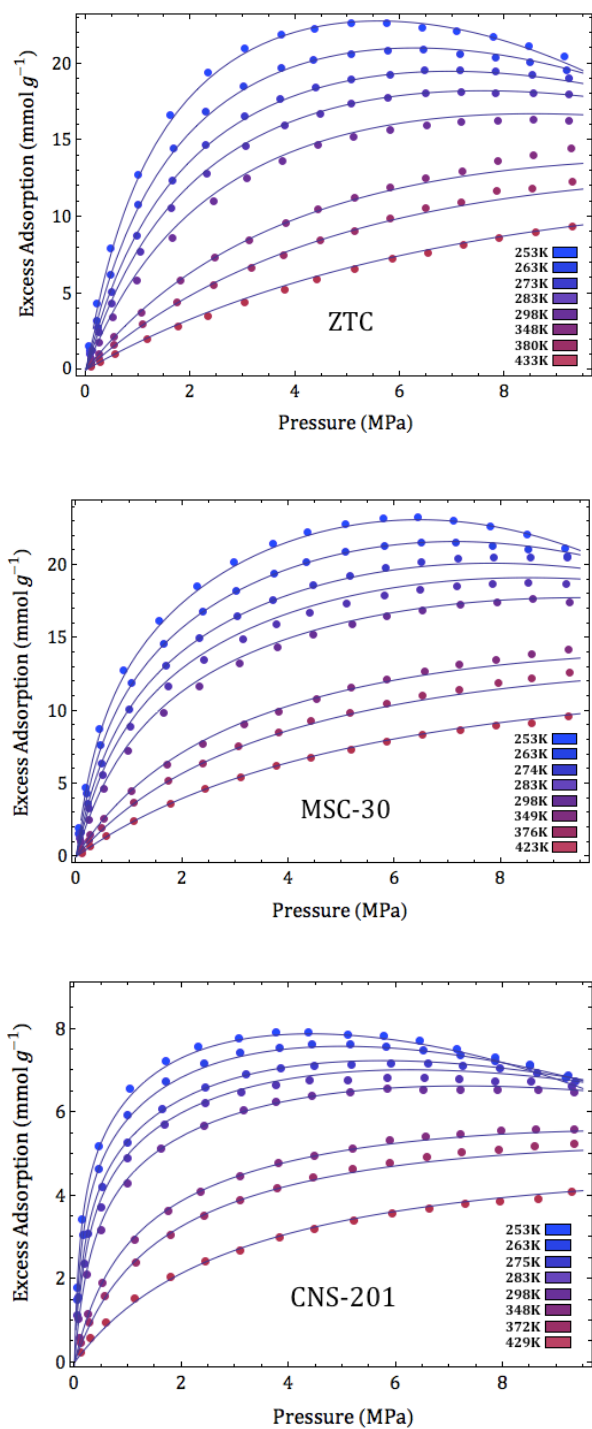


Figure 2. Equilibrium excess adsorption isotherms of krypton on ZTC, MSC-30, and CNS-201. The lines indicate the best fit as determined using a generalized (two-site) Langmuir isotherm model.

4. Data Analysis

4.1 Fitting Methodology

Thermodynamic analysis requires fitting the adsorption data points to a continuous function. While it is common to assume that excess adsorption is equivalent to absolute adsorption at low pressures, this assumption becomes invalid at high pressures and low temperatures. Our method for both fitting and determining the absolute quantity of adsorption from experimental data is based on a generalized-Langmuir model. Briefly, a previously described method³⁹ has been further modified to account for phenomena that are relevant to the nonideal gas regime; the complete details of this methodology are described elsewhere.⁴⁰

Gibbs excess adsorption (n_e) is a function of both the absolute adsorption (n_a) and the gas density in the bulk phase (ρ):

$$n_e = n_a - V_a \rho \quad (1)$$

If the volume of the adsorption layer (V_a) is known, determining absolute adsorption is trivial (given excess adsorption). However, as there is no generally accurate method for determining V_a we have left it as an independent fitting parameter. Excess adsorption quantities were fitted with the following generalized (multisite) Langmuir isotherm:

$$n_e(P, T) = (n_{max} - V_{max} \rho(P, T)) \left[\sum_i \alpha_i \frac{K_i P}{1 + K_i P} \right] \quad (2)$$

Here the independent fitting parameters are n_{max} , the maximum absolute adsorption which serves as a scaling factor, V_{max} which scales with coverage up to the maximum volume of the adsorption layer (V_{max}), α_i which weights the i^{th} Langmuir isotherm ($\sum_i \alpha_i = 1$), and K_i the

equilibrium constant of the i^{th} Langmuir isotherm. K_i is given by an Arrhenius-type equation

where A_i is a prefactor and E_i is the binding energy of the i th Langmuir isotherm:

$$K_i = \frac{A_i}{\sqrt{T}} e^{-E_i/RT} \quad (3)$$

Pressure and temperature are denoted by P and T respectively. By setting the number of Langmuir isotherms equal to two ($i=2$) we limit the number of independent fitting parameters to seven while still obtaining highly accurate fits. The residual mean square values of the fits on ZTC, MSC-30, and CNS-201 are 0.067, 0.070, and 0.0078 (mmol g^{-1})² respectively. Individual fitting parameters for adsorption on the three materials are given in Table 1.

Table 1. Least Squares Minimized Fitting Parameters of Krypton Excess Adsorption

	n_{max} (mmol g ⁻¹)	V_{max} (cm ³ g ⁻¹)	α_1	A_1 (K ^{1/2} MPa ⁻¹)	A_2 (K ^{1/2} MPa ⁻¹)	E_1 (kJ mol ⁻¹)	E_2 (kJ mol ⁻¹)
ZTC	39	2.0	0.31	0.092	1.8E-6	10	30
MSC-30	58	3.0	0.73	0.11	0.0031	12	13
CNS-201	11	0.49	0.46	0.0059	0.069	15	16

The optimized fit parameters were found to be in reasonable agreement with independent estimates of physical quantities. For example, V_{max} corresponds to the maximum micropore filling volume. Dividing V_{max} by the BET surface area of the adsorbent gives an average maximum adsorption layer width. For ZTC, CNS-201, and MSC-30, the maximum adsorption layer widths determined from V_{max} are 5.6, 4.5, and 9.2 Å. These are in reasonable agreement with the average micropore half-widths for ZTC, CNS-201, and MSC-30 as determined by NLDFT analysis of the nitrogen adsorption uptake at 77K, which are 6, 4, and

7 Å, respectively. Additionally, estimates of the maximum possible absolute adsorption can be made by multiplying the measured micropore volume by the density of liquid krypton (28.9 mmol cm⁻³)²². For each material, n_{max} was within 30% of the estimated maximum possible absolute adsorption.

4.2 Determination of Isothermic Enthalpy of Adsorption

The isothermic enthalpy of adsorption (ΔH_{ads}) is a commonly used metric for assessing the strength of adsorbent-adsorbate interactions at constant coverage conditions. Here it is evaluated via the isothermic method and reported as a positive value, q_{st} the isothermic heat defined by the Clapeyron equation:

$$q_{st} = -\Delta H_{ads} = -T \left(\frac{\partial P}{\partial T} \right)_{n_a} (\Delta v_{ads}) \quad (4)$$

The molar change in volume of the adsorbate upon adsorption (Δv_{ads}) is determined by taking the difference between the gas-phase molar volume and the average adsorbed-phase molar volume (the average is approximated as $\frac{V_{max}}{n_{max}}$). The isothermic heats of krypton adsorption on

ZTC, MSC-30, and CNS-201 calculated in this way are shown in Figure 3.

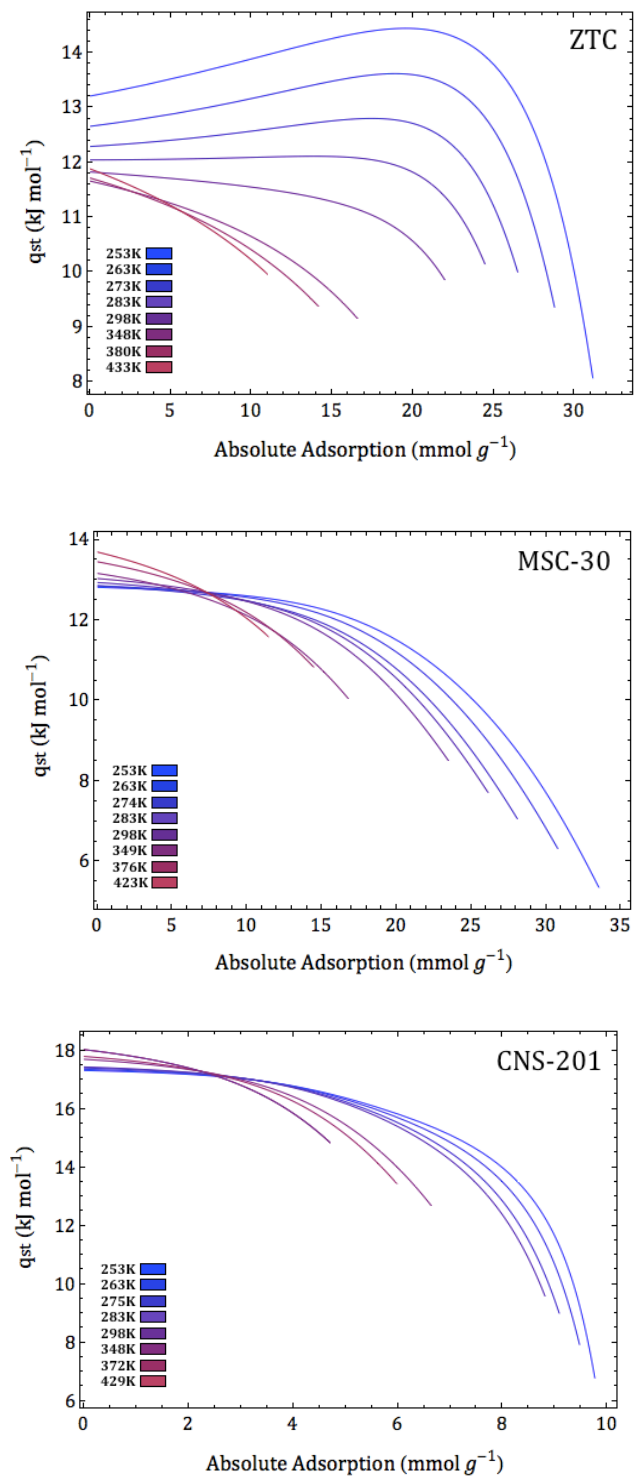


Figure 3. Isosteric heats of krypton adsorption on ZTC, MSC-30, and CNS-201.

5. Discussion

5.1 Isotheric Heat of Adsorption

The isotheric heats of krypton adsorption on MSC-30 and CNS-201 decrease as a function of absolute adsorption, or equivalently surface coverage, as shown in Figure 3. This is the typical behavior of gas adsorption on a heterogeneous surface, where binding sites are filled according to energetic favorability. CNS-201 has significantly higher isotheric heat of adsorption Henry's Law (zero coverage) values due to its small average pore width (8 Å). Krypton adsorption on ZTC, however, is accompanied by an initially increasing isotheric heat with coverage. At 253 K the isotheric heat rises to 14.6 kJ mol^{-1} , 1.4 kJ mol^{-1} above its Henry's Law value of 13.2 kJ mol^{-1} (an 11% increase). This effect has also been observed in both ethane and methane adsorption investigations on ZTC.^{19,20} The increasing isotheric heat is a result of adsorbate-adsorbate interactions promoted by the nanostructured surface of ZTC, an effect that becomes larger at low temperatures. As temperature is increased, the effect is severely diminished. At temperatures above 300 K no increase in the isotheric heat is observed. This suggests that the adsorbate-adsorbate interactions responsible for the increasing isotheric heat of adsorption have cooperative behavior that can be thermally disrupted.

5.2 Slope of Increasing Isotheric Heat of Adsorption

The slope of the increasing isotheric heat as a function of fractional coverage roughly scales with the strength of the intermolecular interactions, as determined by fundamental metrics such as the critical temperature (CT), boiling point (BP), and the Lennard-Jones well depth (ϵ). For krypton, methane, and ethane on ZTC, the average slopes of the isotheric heat

up to 50% surface coverage are reported alongside the CT, BP, and ε parameters for each gas (see Table 2).

Table 2. Slopes of Isothermic Heats of Adsorption as a Function of Fractional Coverage on ZTC at the Lowest Measured Temperature and Gas Properties of Krypton, Methane, and Ethane.

	Slope (kJ mol ⁻¹)	CT (K)	BP (K)	ε (kJ mol ⁻¹)
Krypton	2.7	209 ²²	120 ²²	1.3 ²¹
Methane	2.2	190 ²²	112 ²²	1.2 ²¹
Ethane	3.3	305 ²²	185 ²²	1.7 ⁴¹

The ratios of the krypton/methane and krypton/ethane slopes are 1.2 and 0.82 respectively. These ratios are similar to the krypton/methane and krypton/ethane ratios of CT, BP, and ε . Furthermore, the slopes of the isothermic heat are in good agreement with a simplistic model that we have previously proposed¹⁹:

$$\frac{\partial(\xi)}{\partial\theta} = \frac{z\varepsilon}{2} \quad (5)$$

The left hand side of Equation 5 ($\frac{\delta(\xi)}{\delta\theta}$) is the slope of the isothermic heat as a function of fractional coverage while z represents the number of nearest neighbors (posited to be 4) and ε is the Lennard-Jones potential well depth of the gas. Using Equation 5 the slopes of the krypton, methane and ethane isothermic heats on ZTC are estimated to be 2.6, 2.4, and 3.4 kJ mol⁻¹ (all within 10 percent of the average measured slope for each gas).

5.3 Isothermic Heat of Adsorption Maxima

At high coverage the isothermic heat of krypton adsorption on ZTC reaches a maximum and decreases with further coverage. In this regime the adsorbed-phase interatomic interactions are dominated by short-range repulsion due to the high density of adsorbates. The

optimal density for promoting adsorbate-adsorbate interactions is the adsorbate density at the maximum of the isosteric heat (for a given temperature). Here we label this optimal adsorbate density “ $\rho\Delta H_{max}$ ” and make comparisons to the bulk gas phase via the compressibility factor (Z). The compressibility factor provides a good metric of the nonideality of a gas under specific conditions.

$$Z = \frac{PV}{nRT} \quad (6)$$

While an ideal gas has a compressibility factor of 1, attractive intermolecular interactions decrease Z and repulsive interactions increase Z . For a van der Waals gas, the compressibility factor can be recast in terms of the coefficients of the van der Waals equation of state (a and b):

$$Z = \frac{V}{V-nb} - \frac{an}{RTV} \quad (7)$$

In this representation the minimum of the compressibility factor (where attractive interactions are most dominant) occurs at:

$$n = \frac{V - \left(\frac{V^2 b R T}{a}\right)^{\frac{1}{2}}}{b} \quad (8)$$

As temperature is increased at a fixed volume (V), the minimum point of the compressibility factor shifts to a lower number of particles (n) and hence to a lower density. The actual compressibility factor of krypton²² shows similar behavior (see Figure 4).

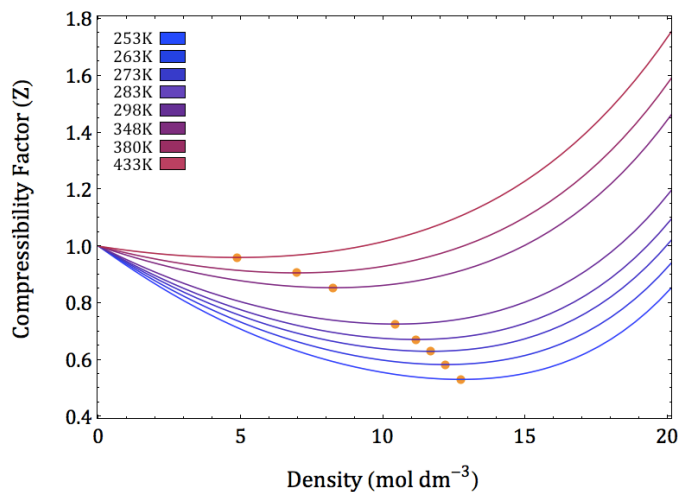


Figure 4. Compressibility factor of krypton between 253-433 K, as calculated by REFPROP²². The minima are indicated by orange circles.

The importance of the minimum in the compressibility factor is that it represents a critical point after which repulsive interactions begin to dominate over attractive interactions in the gas. The density at the compressibility factor minimum (ρZ_{min}), shown in Figure 4, can therefore be expected to correlate with the density of the adsorbed phase at the maximum in isosteric heat of adsorption ($\rho \Delta H_{max}$). Low temperature values (253-273 K) of $\rho \Delta H_{max}$ (for krypton on ZTC) were determined by dividing the absolute adsorption quantity at the isosteric heat maximum by the ZTC micropore volume ($1.66 \text{ cm}^3 \text{ g}^{-1}$). There is reasonable agreement between ρZ_{min} and $\rho \Delta H_{max}$ at low temperatures (less than 12% discrepancy) (see Figure 5).

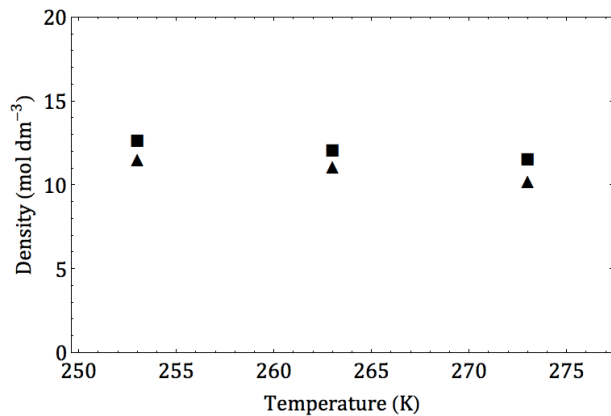


Figure 5. Comparison of ρZ_{min} (squares) and $\rho \Delta H_{max}$ (triangles).

5.4 Adsorbed-Phase Enthalpy

The adsorbed-phase enthalpy (H_a) of krypton on ZTC, MSC-30, and CNS-201 was determined as a function of coverage by adding the isosteric enthalpy of adsorption to the gas-phase enthalpy (H_g) (determined by REFPROP²²) (see Figure 6).

$$H_a = H_g + \Delta H_{ads} \quad (9)$$

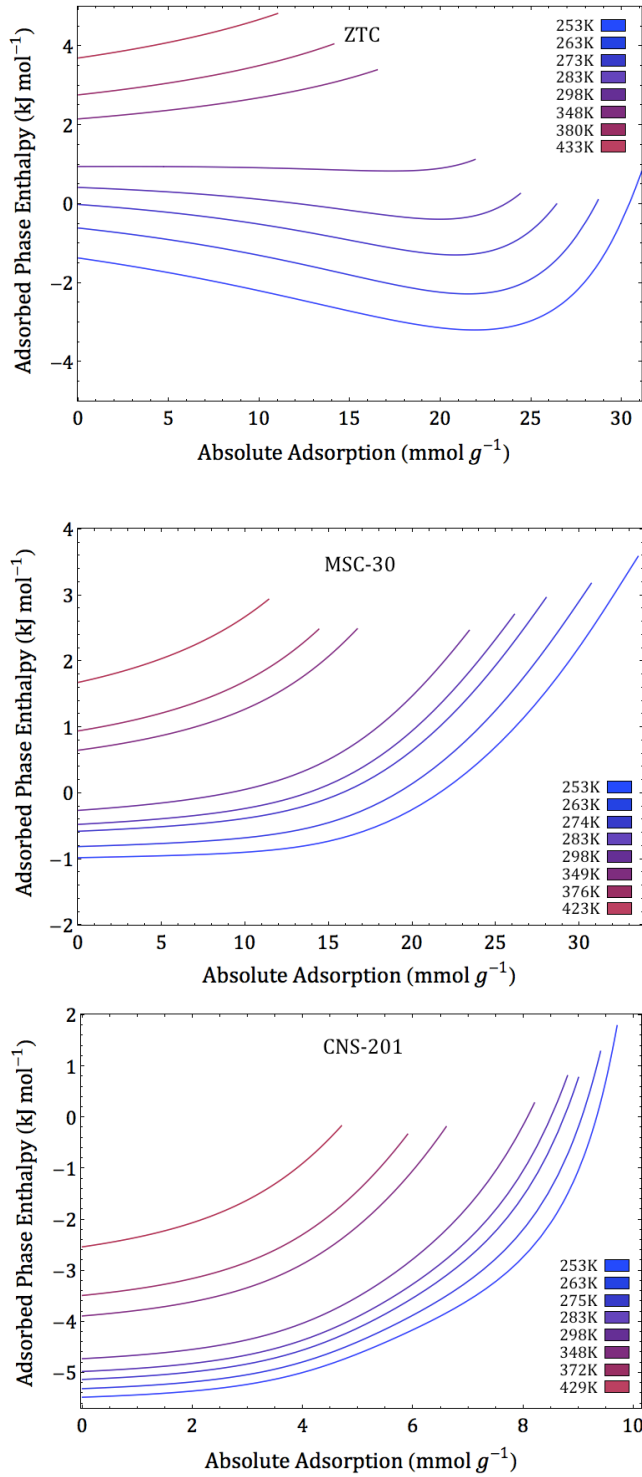


Figure 6. Adsorbed-phase enthalpy of krypton on ZTC, MSC-30, and CNS-201.

Due to favorable adsorbate-adsorbate interactions, the adsorbed-phase enthalpy of krypton on ZTC decreases towards a minimum (most favorable) enthalpy with coverage. Conversely, the adsorbed-phase enthalpy of krypton on MSC-30 and CNS-201 increases with coverage. The adsorbed-phase enthalpy may also be determined as a function of average interatomic distance. For example, the average interatomic distance of adsorbed krypton (x_{avg}) at a given state of surface coverage can be determined by dividing the micropore volume, V_{mic} , (1.66 cm³ g⁻¹ for ZTC) by the quantity of absolute adsorption (n_a), and taking the cube root:

$$x_{avg} = \left(\frac{V_{mic}}{n_a} \right)^{\frac{1}{3}} \quad (10)$$

The adsorbed-phase enthalpy at 253 K on ZTC as a function of average interatomic distance is comparable to the 12-6 Lennard-Jones potential between two krypton atoms²¹ (see Figure 7).

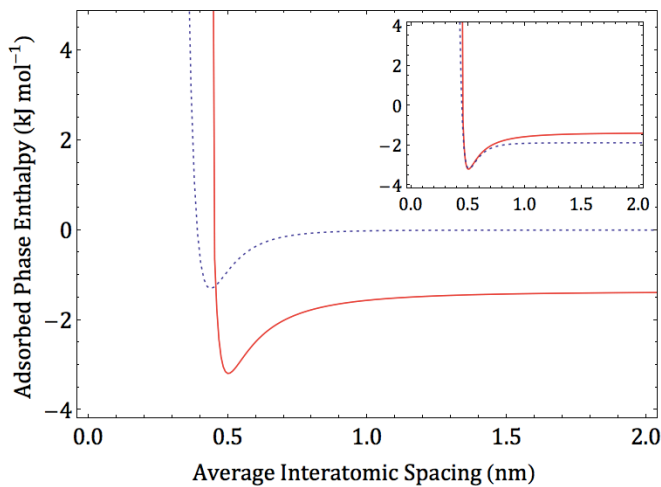


Figure 7. Comparison of the adsorbed-phase enthalpy of krypton on ZTC at 253 K (red) and the 12-6 Lennard-Jones potential of krypton (dashed blue). The inset shows both curves translated and superimposed for easier comparison.

At the lowest measured temperature in this work (253 K), the magnitude and form of the adsorbed-phase enthalpy of krypton on ZTC is remarkably similar to the 12-6 Lennard-Jones potential. Conversely, the adsorbed-phase enthalpies of krypton on MSC-30 and CNS-201 display no such behavior and are monotonically increasing functions. This provides further evidence that the anomalous isosteric heat of adsorption of krypton on ZTC results from enhanced interatomic interactions which can be rather accurately accounted for by the classic 12-6 interaction potential. The apparent offset in energy seen in Figure 7 is a result of the adsorbent-adsorbate interactions and the arbitrary nature of the enthalpy reference state (in this case the reference state is saturated liquid krypton at its normal boiling point, 120 K). The offset in interatomic distance (~ 0.07 nm) between the adsorbed-phase enthalpy and the 12-6 Lennard-Jones potential may result from clustering of the krypton atoms. While some of the krypton atoms may temporarily cluster into more optimally spaced groupings which reproduce the 12-6 Lennard-Jones potential shape and distance, the presence of non-clustered krypton atoms with larger interatomic distances could shift the *average* interatomic spacing to higher values resulting in the offset in interatomic distance.

The Henry's Law values of the adsorbed-phase enthalpies are also indicative of the atypical properties of ZTC as an adsorbent for krypton. The enthalpy of a two-dimensional ideal gas is $2RT$ and therefore depends linearly on temperature with a slope of $2R$ ($16.6 \text{ J mol}^{-1} \text{ K}^{-1}$). Correspondingly, the Henry's Law values of the adsorbed-phase enthalpy of krypton on MSC-30 and CNS-201 also depend linearly on temperature, with slopes of 15.6 and $16.7 \text{ J mol}^{-1} \text{ K}^{-1}$, respectively (see Figure 8).

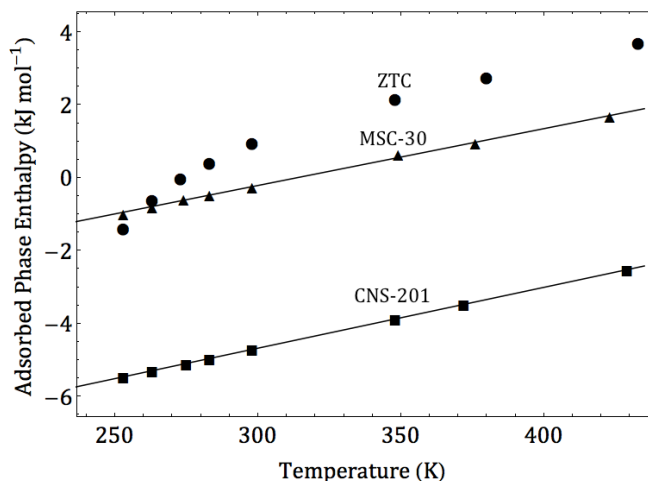


Figure 8. Henry's law enthalpies of adsorbed krypton on ZTC (circles), MSC-30 (triangles) and CNS-201 (squares) as a function of temperature. Lines are to guide the eye.

The Henry's Law values of the adsorbed-phase enthalpy of krypton on ZTC, however, do not vary linearly with temperature until beyond 350 K. At high temperatures (>350 K) the slope converges to approximately $2R$. At low temperatures, however, deviations between the measured Henry's Law values and those predicted using the ideal gas slope of $2R$, are observed. These deviations likely result from the unique structure of ZTC and may in part be due to a loss of favorable interactions with increasing temperature.

5.5 Entropy

The isosteric entropy of adsorption (ΔS_{ads}) is the change in entropy upon adsorption: the difference between the entropy of the adsorbed phase and the entropy of the gas phase at isosteric conditions. At equilibrium, the isosteric entropy of adsorption and the isosteric enthalpy of adsorption (ΔH_{ads}) are related by:

$$\Delta S_{ads} = \frac{\Delta H_{ads}}{T} \quad (13)^{19}$$

As for the enthalpy, the entropy of the adsorbed phase can be determined by adding the isosteric entropy of adsorption to the entropy of krypton gas (calculated using REFPROP²²). The molar entropy of adsorbed-phase krypton as a function of coverage on the three materials in this study is shown in Figure 9. The reference state in this case is solid krypton at absolute zero.

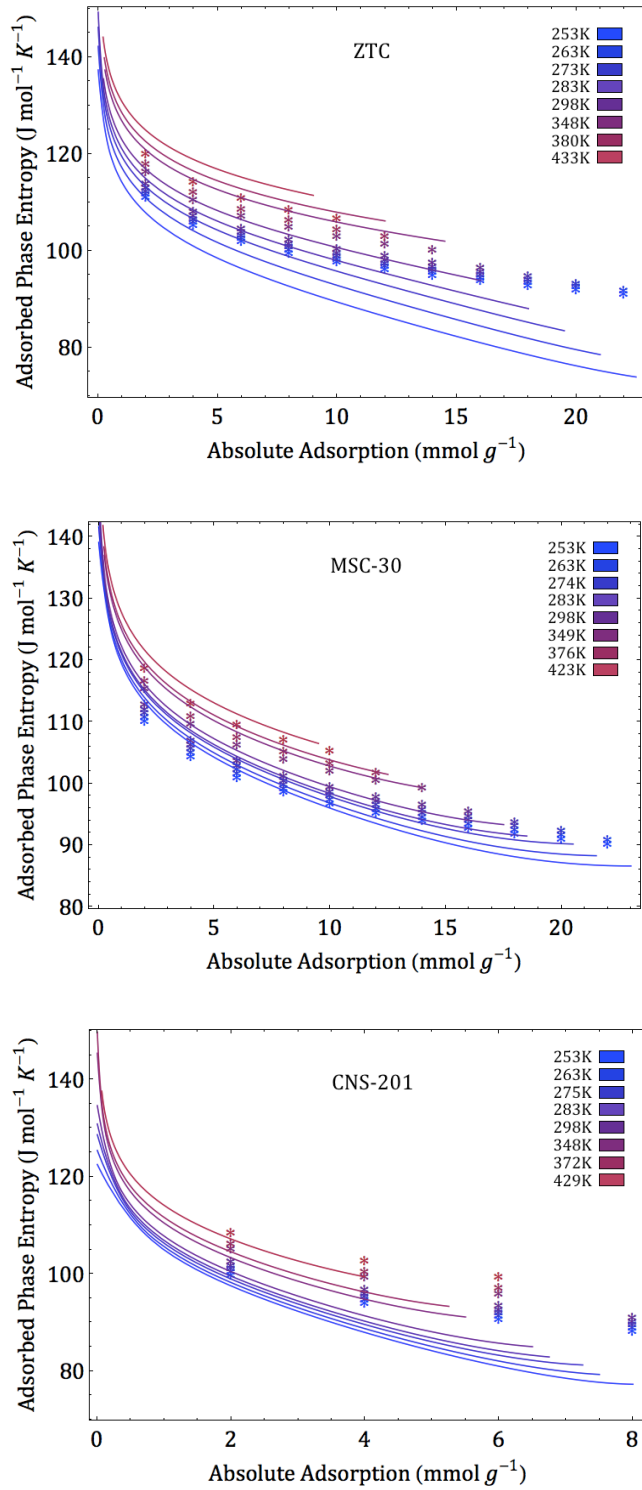


Figure 9. The entropy of adsorbed-phase krypton on ZTC, MSC-30 and CNS-201 derived by experiment (lines) and calculated using statistical mechanics (asterisks).

For comparison to the experimental data, the adsorbed-phase entropy of krypton was also calculated using statistical mechanics (shown in Figure 9). A basic statistical mechanics model based on a two-dimensional lattice gas was used, as described elsewhere¹⁹. Since krypton is a monatomic gas with spherical symmetry and no internal vibrational modes, only partition functions for the surface vibrational modes and configurational modes were considered. The entropies corresponding to these individual contributions were determined and summed to obtain the total entropy of the adsorbed phase (see Figure 9).

For krypton adsorbed on MSC-30 and CNS-201, agreement between the measured and calculated adsorbed-phase entropies is good, with discrepancies of 5% and 15% respectively. The small pores and high isosteric heat of adsorption of krypton on CNS-201 result in less accurate statistical mechanics approximations of surface vibrational modes and hence somewhat larger deviations than for MSC-30. Moreover, the general temperature dependence is preserved in both cases, especially at low quantities of uptake. For krypton on ZTC, however, discrepancies are in excess of 23% despite moderate pore sizes; the experimental adsorbed-phase entropy is much lower than estimated values due to enhanced interatomic interactions. It is reasonable to attribute a large fraction of this discrepancy to clustering effects (reduced configurations of the adsorbed phase due to interatomic interactions)⁴⁰, and further investigation of such phenomena is warranted.

6. Conclusions

Equilibrium excess adsorption uptake of krypton was measured on three microporous carbon materials: ZTC, MSC-30 and CNS-201. By fitting the data using a robust generalized Langmuir isotherm model, absolute adsorption quantities were determined along with

physically realistic fitting parameters and thermodynamic quantities of adsorption. While the isosteric heat of adsorption decreases with coverage on MSC-30 and CNS-201 (the typical case), it increases by over 10% on ZTC, reaching its maximum at a surface coverage of 19.6 mmol g⁻¹ at 253 K. This previously unreported effect for supercritical krypton adsorption on a high surface area carbon results from the enhancement of favorable krypton-krypton interactions on the ZTC surface due to its uniquely ordered porous nanostructure. Moreover, the magnitude of the increase is dependent on the strength of the interatomic interactions of krypton, a result that is corroborated by comparisons to ethane and methane. Additional analysis of the isosteric heat of adsorption maxima, adsorbed-phase enthalpy, and adsorbed-phase entropy provide further evidence and insight into the nature of the interactions responsible for the anomalous surface thermodynamics reported in this paper.

Acknowledgement:

This work was sponsored as a part of EFree (Energy Frontier Research in Extreme Environments), an Energy Frontier Research Center funded by the US Department of Energy, Office of Science, Basic Energy Sciences under Award Number DE-SC0001057.

References:

1. Dillon, A. C.; Heben, M. J. Hydrogen Storage Using Carbon Adsorbents: Past, Present and Future. *Appl. Phys. A: Mater. Sci. Process.* **2001**, *72*, 133-142.
2. Richard, M. A.; Cossement, D.; Chandonia, P. A.; Chahine, R.; Mori, D.; Hirose, K. Preliminary Evaluation of the Performance of an Adsorption-Based Hydrogen Storage System. *AIChE J.* **2009**, *55*, 2985-2996.
3. Alcaniz-Monge, J.; Lozano-Castello, D.; Cazorla-Amoros, D.; Linares-Solano, A. Fundamentals of Methane Adsorption in Microporous Carbons. *Microporous Mesoporous Mater.* **2009**, *124*, 110-116.
4. Dabrowski, A. Adsorption - from Theory to Practice. *Adv. Colloid Interface Sci.* **2001**, *93*, 135-224.
5. Panella, B.; Hirscher, M.; Roth, S. Hydrogen Adsorption in Different Carbon Nanostructures. *Carbon* **2005**, *43*, 2209-2214.
6. Poirier, E.; Chahine, R.; Bose, T. K. Hydrogen Adsorption in Carbon Nanostructures. *Int. J. Hydrogen Energy* **2001**, *26*, 831-835.
7. Plaza, M. G.; Pevida, C.; Arenillas, A.; Rubiera, F.; Pis, J. J. CO₂ Capture by Adsorption with Nitrogen Enriched Carbons. *Fuel* **2007**, *86*, 2204-2212.
8. Samanta, A.; Zhao, A.; Shimizu, G. K. H.; Sarkar, P.; Gupta, R. Post-Combustion CO₂ Capture Using Solid Sorbents: A Review. *Ind. Eng. Chem. Res.* **2012**, *51*, 1438-1463.
9. Kyotani, T.; Nagai, T.; Inoue, S.; Tomita, A. Formation of New Type of Porous Carbon by Carbonization in Zeolite Nanochannels. *Chem. Mater.* **1997**, *9*, 609-615.
10. Ryoo, R.; Joo, S. H.; Kruk, M.; Jaroniec, M. Ordered Mesoporous Carbons. *Adv. Mater.* **2001**, *13*, 677-681.
11. Nishihara, H.; Kyotani, T. Templated Nanocarbons for Energy Storage. *Adv. Mater.* **2012**, *24*, 4473-4498.
12. Yang, Z. X.; Xia, Y. D.; Mokaya, R. Enhanced Hydrogen Storage Capacity of High Surface Area Zeolite-Like Carbon Materials. *J. Am. Chem. Soc.* **2007**, *129*, 1673-1679.
13. Nishihara, H.; Hou, P.-X.; Li, L.-X.; Ito, M.; Uchiyama, M.; Kaburagi, T.; Ikura, A.; Katamura, J.; Kawarada, T.; Mizuuchi, K.; Kyotani, T. High-Pressure Hydrogen Storage in Zeolite-Templated Carbon. *J. Phys. Chem. C* **2009**, *113*, 3189-3196.
14. Yang, Z. X.; Xia, Y. D.; Sun, X. Z.; Mokaya, R. Preparation and Hydrogen Storage Properties of Zeolite-Templated Carbon Materials Nanocast via Chemical Vapor Deposition: Effect of the Zeolite Template and Nitrogen Doping. *J. Phys. Chem. B* **2006**, *110*, 18424-18431.
15. Su, F. B.; Zhao, X. S.; Lv, L.; Zhou, Z. C. Synthesis and Characterization of Microporous Carbons Templated by Ammonium-Form Zeolite Y. *Carbon* **2004**, *42*, 2821-2831.
16. Xia, Y. D.; Mokaya, R.; Walker, G. S.; Zhu, Y. Q. Superior CO₂ Adsorption Capacity on N-doped, High-Surface-Area, Microporous Carbons Templated from Zeolite. *Adv. Energy Mater.* **2011**, *1*, 678-683.
17. Guan, C.; Su, F. B.; Zhao, X. S.; Wang, K. Methane Storage in a Template-Synthesized Carbon. *Sep. Purif. Technol.* **2008**, *64*, 124-126.

18. Kyakuno, H.; Matsuda, K.; Nakai, Y.; Fukuoka, T.; Maniwa, Y.; Nishihara, H.; Kyotani, T. Amorphous Water in Three-Dimensional Confinement of Zeolite-Templated Carbon. *Chem. Phys. Lett.* **2013**, *571*, 54-60.
19. Murialdo, M.; Stadie, N. P.; Ahn, C. C.; Fultz, B. Observation and Investigation of Increasing Isothermic Heat of Adsorption of Ethane on Zeolite-Templated Carbon. *J. Phys. Chem. C* **2015**, *119*, 944-950.
20. Stadie, N. P.; Murialdo, M.; Ahn, C. C.; Fultz, B. Anomalous Isothermic Enthalpy of Adsorption of Methane on Zeolite-Templated Carbon. *J. Am. Chem. Soc.* **2013**, *135*, 990-993.
21. Cuadros, F.; Cachadina, I.; Ahumada, W. Determination of Lennard-Jones Interaction Parameters Using a New Procedure. *Mol. Eng.* **1996**, *6*, 319-325.
22. Lemmon, E. W.; Huber, M. L.; McLinden, M. O. *NIST Standard Reference Database 23: Reference Fluid Thermodynamic and Transport Properties-REFPROP*, version 8.0; National Institute of Standards and Technology: Gaithersburg, MD, 2007; CD-ROM.
23. Hwang, H. S.; Baik, H. K.; Park, K. W.; Song, K. M.; Lee, S. J. Excitation Energy Transfer of Metastable Krypton Atoms in Kr-He-Xe Low Pressure Glow Discharge for Mercury-Free Lighting. *Jpn. J. Appl. Phys.* **2010**, *49*, 3.
24. Chon, D.; Beck, K. C.; Simon, B. A.; Shikata, H.; Saba, O. I.; Hoffman, E. A. Effect of Low-Xenon and Krypton Supplementation on Signal/Noise of Regional CT-based Ventilation Measurements. *J. Appl. Physiol.* **2007**, *102*, 1535-1544.
25. Pavlovskaya, G. E.; Cleveland, Z. I.; Stupic, K. F.; Basaraba, R. J.; Meersmann, T. Hyperpolarized Krypton-83 as a Contrast Agent for Magnetic Resonance Imaging. *Proc. Natl. Acad. Sci. U.S.A.* **2005**, *102*, 18275-18279.
26. Takei, T.; Chikazawa, M. Measurement of Pore Size Distribution of Low-Surface-Area Materials by Krypton Gas Adsorption Method. *J. Ceram. Soc. Jpn.* **1998**, *106*, 353-357.
27. Youssef, A. M.; Bishay, A. F.; Hammad, F. H. Determination of Small Surface-Areas by Krypton Adsorption. *Surf. Technol.* **1979**, *9*, 365-370.
28. Ryan, P.; Farha, O. K.; Broadbelt, L. J.; Snurr, R. Q. Computational Screening of Metal-Organic Frameworks for Xenon/Krypton Separation. *AIChE J.* **2011**, *57*, 1759-1766.
29. Bae, Y.-S.; Hauser, B. G.; Colon, Y. J.; Hupp, J. T.; Farha, O. K.; Snurr, R. Q. High Xenon/Krypton Selectivity in a Metal-Organic Framework with Small Pores and Strong Adsorption Sites. *Microporous Mesoporous Mater.* **2013**, *169*, 176-179.
30. Izumi, J. Waste Gas Treatment Using Zeolites in Nuclear-related Industries. In *Handbook of Zeolite Science and Technology*; Auerbach, S. M., Carrado, K. A., Dutta, P. K., Eds.; Marcel Dekker: New York, 2003; Chapter 20.
31. Stadie, N. P.; Vajo, J. J.; Cumberland, R. W.; Wilson, A. A.; Ahn, C. C.; Fultz, B. Zeolite-Templated Carbon Materials for High-Pressure Hydrogen Storage. *Langmuir* **2012**, *28*, 10057-10063.
32. Dubinin, M. M.; Radushkevich, L. V. Equation of the Characteristic Curve of Activated Charcoal. *Proc. Acad. Sci. USSR, Phys. Chem. Sect.* **1947**, *55*, 331-337.
33. Nguyen, C.; Do, D. D. The Dubinin-Radushkevich Equation and the Underlying Microscopic Adsorption Description. *Carbon* **2001**, *39*, 1327-1336.

34. Brunauer, S.; Emmett, P. H.; Teller, E. Adsorption of Gases in Multimolecular Layers. *J. Am. Chem. Soc.* **1938**, *60*, 309-319.
35. Lastoskie, C.; Gubbins, K. E.; Quirke, N. Pore-Size Distribution Analysis of Microporous Carbons - A Density-Functional Theory Approach. *J. Phys. Chem.* **1993**, *97*, 4786-4796.
36. Lastoskie, C.; Gubbins, K. E.; Quirke, N. Pore-Size Heterogeneity and the Carbon Slit Pore - A Density-Functional Theory Model. *Langmuir* **1993**, *9*, 2693-2702.
37. Bowman, R. C.; Luo, C. H.; Ahn, C. C.; Witham, C. K.; Fultz, B. The Effect of Tin on the Degradation of LaNi_{5-y}Sny Metal-Hydrides During Thermal Cycling. *J. Alloys Compd.* **1995**, *217*, 185-192.
38. Sircar, S. Gibbsian Surface Excess for Gas Adsorption - Revisited. *Ind. Eng. Chem. Res.* **1999**, *38*, 3670-3682.
39. Mertens, F. O. Determination of Absolute Adsorption in Highly Ordered Porous Media. *Surf. Sci.* **2009**, *603*, 1979-1984.
40. Stadie, N. P.; Murialdo, M.; Ahn, C. C.; Fultz, B. Unusual Thermodynamics and Clustering of Adsorbed Methane on Zeolite-Templated Carbon. *J. Phys. Chem. C*, submitted for publication, **2015**.
41. Tee, L. S.; Gotoh, S.; Stewart, W. E. Molecular Parameters for Normal Fluids - Lennard-Jones 12-6 Potential. *Ind. Eng. Chem. Fundam.* **1966**, *5*, 356-363.